Volume 1 | Number 1 | Jan 2013 | Pages 1–100

Journal of
**Materials Chemistry A**

Materials for energy and sustainability
www.rsc.org/materialsA

Li⁺

ROYAL SOCIETY
OF CHEMISTRY

ROYAL SOCIETY
OF CHEMISTRY

www.rsc.org/materialsA

**ARTICLE TYPE**

# Nitrogen-doped Activated Carbons Derived from Co-Polymer for High Supercapacitor Performance

**Akram Alabadi,[a,b] Xinjia Yang,[a] Zehua Dong,[a] Zhen Li[c] and Bien Tan\*[a]**

Nitrogen-doped activated carbons (N-ACs) with controlled nitrogen doping and analogous microporous structures were prepared by the pyrolysis of poly [(pyrrole-2, 5-diyl)-co-(benzylidene)] (PPCB). The obtained N-ACs were thoroughly characterized using HRTEM, FESEM, BET, FTIR and XPS for their morphology, surface area and chemical composition. The N-ACs were further used to fabricate
10 supercapacitors, and their comprehensive electrochemical properties, such as cyclic voltammetry, galvanostatic charge/discharge, electrochemical impedance spectrum, electrochemical capacitive performance, power density and long cyclic stability were studied. The galvanostatic charge/discharge (GC) measurements on N-ACs produced at 700˚C and 800˚C show a high specific capacitance (up to 525.5 F g$^{-1}$ and energy density ca. 262.7 W h kg$^{-1}$ at 0.26 A g$^{-1}$) in alkaline media (2M KOH). More
15 importantly, the capacitance remains practically identical when the scanning rate was increased from 0.26 to 26.31 A g$^{-1}$. The observed capacitance retention (~ 99.5%) of N-ACs is remarkably stable for electrodes even after 4000 cycles, due to the presence of nitrogen at the surface and in the graphitic edge planes. The nitrogen content plays a significant role to produce micropores dominated ACs and to facilitate the transfer of the ions through pores on the surface. The precursor (PPCB) used is cheap and
20 can easily be prepared, making it promising for the large scale production of N-ACs as an excellent electrode material for supercapacitors.

## Introduction

Currently there is a high demand to produce inexpensive, lightweight, adaptable, environmental friendly and more efficient
25 energy storage devices. Due to the obvious reasons, the energy storage materials act as key building blocks for energy-conversion devices.[1, 2] Consequently, research is being conducted to produce robust, efficient and flexible electrode materials to replace the materials used in supercapacitors and contemporary
30 batteries.[3] Supercapacitors, also known as Electric Double-Layer Capacitors (EDLCs), have been used as energy-storage devices and as auxiliary power sources in composition of batteries, which promise large power density, stable cycle life and high cycle efficiency.[4]

35 In EDLCs, porous carbon materials with high surface area are usually used as electrode materials including microporous carbide-derived carbons, [5] mesoporous carbons and activated carbons (ACs).[6, 7] The accumulation of energy is completed through isolation of ionic charges on the electrode–electrolyte
40 interface. The high specific capacitance of carbon materials depends on several key factors such as high specific surface area, suitable pore size and existence of functional groups present heteroatoms that enhance the interaction between the ionic charge and the carbon surface.[8] Generally, large surface area of carbon-
45 based materials leads to an increase in their capacitance.

Moreover, the pore size also needs to be compatible with the radius of the ions from electrolytes and the existing functional groups or heteroatoms on the surface of carbon materials to
50 achieve remarkably high specific capacitance of carbon materials.[9]

On the other hand, conductive polymers or polymers containing heteroatoms for instance polyaniline,[10] polypyrrole (PPy), polythiophene and their derivatives have also attracted
55 considerable attention to fabricate supercapacitors with useful properties, such as high charge density, large doping-dedoping range in charge-discharge processes, and easy synthesis by chemical or electrochemical methods.[11] Among these polymers, PPy is one of the most widely studied conductive polymers due to
60 many advantages including high electrical conductivity, easier preparation, perfect redox activity and better environmental stability.[12-14] It has also inspired researchers interest for their numerous technological applications, such as sensors, rechargeable batteries or electric devices etc.[15] Although, PPy
65 often possesses positive charges during polymerization, it is usually substituted by incorporation of anions in the polymer chains.[16] Up to date, conductive polymers have been used as electrochemically active materials for supercapacitors and pseudo-capacitors, but their practical applications are still under
70 exploration. Therefore, it has become extremely necessary to

speed up the efforts to produce economical and more effective electrode materials possessing high power and large energy densities.[17]

Currently, to search the optimal electrode materials for supercapacitors, there is an increasing trend to combine more than one materials through blending *e.g.* graphene or graphene oxide (GO) with polymers,[18, 19] or co-polymerization of monomers.[20] Since the technique of electrochemical analysis of structural and chemical properties of porous carbon materials have limited forecasting abilities, most of the studies have announced important impacts of structural drawbacks of porous carbon materials on their electro-sorption and increase ion adsorption in pores into selected materials systems.[16, 21] The great challenge comes from the difficultly in regulating different materials characteristics required for orderly experimental studies and from the wide intricacy of the actual material system.

Porous activated carbons (ACs) with large specific surface area have enhanced capacitance for supercapacitor applications.[22] However, irrespective of their high surface area, the presence of heteroatoms on the surface of porous carbon materials has been regarded as an attractive way to increase their capacitance. For instance, nitrogen and sulphur are well known for their basic and electron donating properties and are considered as attractive dopants for porous carbon materials to improve their capacitance.[23, 24]. Moreover, the presence of nitrogen groups also increase the polar and hydrophilic nature of the electrodes surface.[25] Despite the large efforts to synthesise activated carbon-based electrode materials with high power density and high conductivity, the superior performance of supercapacitors still remains a great challenge.[26] Most of the previous studies have established that nitrogen functionalization of porous carbon materials can increase capacitance of the electrode materials. In order to obtain good electrode materials of both high-capacitance and high-rate supercapacitors, less nitrogen-doped porous carbons should be contained.[27]

Many strategies have been conducted to use PPy as supercapacitor electrode materials including their doping with anions, single walled or multi-walled CNTs, micellar deposition, and even their carbonization.[28] Among these strategies, carbonization of PPy has been found to be an appropriate solution to improving the electrochemical properties of electrodes based on super-capacitance materials. The highest specific capacitance of activated PPy is about 354 F g$^{-1}$ obtained from the CV curve at the scan rate of 1 mV s$^{-1}$ and 466 F g$^{-1}$ at 10 mV s$^{-1}$ for a chemically polymerized PPy coated with graphite fibbers.[29] Whereas only 140 F g$^{-1}$ capacitance is recorded for AC by cyclic voltammograms in the three-electrode method after adjusting the total weight of electrode. PPy is a well-known and versatile electrode material, but the recycling instability is its major limitation in supercapacitor applications.[30] However, using PPy composites with other materials such as CNTs and $MnO_2$ improves its recycling stability towards an acceptable recycling life.[31]

In this work, we have examined the relationship between porous structure and chemistry of activated carbons and their electrical energy storage performance. A simple strategy was developed to produce nitrogen-doped activated carbons (N-ACs) based on a conjugated polymer poly [(pyrrole-2,5-diyl)-co-(benzylidene)] (PPCB) as precursor followed by chemical activation with KOH at different temperatures. By this method, nitrogen contents can be controlled by adjusting the carbonization temperature. Moreover, the preparation procedure is simple, and the nitrogen on the carbon framework remains stable even under harsh conditions to produce highly desirable nitrogen-doped carbon materials with appropriate porosity and large electrical conductivity. The obtained N-ACs exhibited uniform micropores and small mesopore size, large surface area (up to 2090 m$^2$ g$^{-1}$) and high nitrogen contents. The change in textural properties and nitrogen characteristics of N-ACs under the synthetic conditions were constantly observed and optimized. Supercapacitors based on nitrogen enriched ACs with alkaline electrolytes showed a much higher specific capacitance and a lower ions diffusion resistance compared to other commonly used ACs. To the best of our knowledge, this is the first report to use PPCB as a precursor to produce N-doped ACs with superior properties for applications in superacapacitors.

## Experimental

### Synthesis

Poly[(pyrrole-2,5-diyl)-co-(benzylidene)](PPCB) and analytic-cal grade KOH (sinopharm chemical reagent co ltd Shanghai. Purity ≥85.0%) were used as precursor and an activating agent, respectively. PPCB was synthesized by the condensation of pyrrole (Aladdin Co. purity ≥98.0%) and benzaldehyde (sinopharm chemical reagent co ltd Shanghai. Purity =98.0%) as monomer in the presence of bentonite Mag-H$^+$ as a catalyst.[32] In a 50 ml round flask, pyrrole (8 mmol), benzaldehyde (8 mmol) and 1g of Mag-H$^+$ were dissolved in 10 ml of 1, 2-dichloroethane. The mixture was heated to 80˚C for 1 h. At the end of reaction, the resulting mixture was filtered and washed with methanol and the polymer was dried under vacuum at room temperature for 24 h. To prepare activated carbon, powdered PPCB was carbonized at 450˚C in a tubular furnace to produce porous carbon (PC). Then PC was mixed evenly with KOH at a desired ratio (1/4) and the mixture was heated in a tubular furnace up to 700˚C or 800˚C at a rate of 10˚C/min and maintained at the desired temperature for 1 h under nitrogen (99.999 %) to achieve carbonization and activation at the same time. The resulting material was then cooled down to room temperature, and the products were taken out and washed with dilute HCl (10 wt%) first and then with distilled water to remove any residual water soluble impurities, followed by drying at 80˚C for 24 h. The final activated carbons obtained with a constant weight ratio of KOH/PPCB were labelled as N-AC-T, where T: refers to the target temperature.

### Characterization

The morphology of the samples was examined by using Field Emission Scanning Electron Microscopy (FE-SEM, SIRION 200) at 5 kV and TECNAI G$^2$ 20 High Resolution Transmission Electron Microscope (HR-TEM) at 200 kV. All HR-TEM samples were prepared by evaporating a drop of dilute suspension of N-ACs in ethanol on a carbon-coated copper grid. FTIR

spectroscopic analysis of N-ACs was carried out using a Bruker Vertex 70 spectrometer For the FTIR measurements, the samples were mixed with potassium bromide (KBr), and then pressed into pellets. The surface elemental composition was determined by the X-ray photoelectron spectroscopy (XPS) technique using AXIS-ULTRA DLD high-performance imaging (Shimadzu, Japan). Raman spectra data was collected on LAB RAM HR800 HORIBA Scientific - France using 522 nm argon laser. In addition, elemental analysis was conducted on a Vario EL cube (Elementar Analysensysteme GmbH) to determine the total carbon and nitrogen content of the samples. The specific surface area and pore size distribution (PSD) of the activated carbons were determined using nitrogen adsorption-desorption isotherms at 77 K (Micromeritics ASAP 2020 surface area and porosity analyzer). Prior to measurement, the samples were degassed under vacuum at 110 ˚C for ca. 12 h until the pressure was less than 5 mmHg. The specific surface area ($S_{BET}$) was calculated by the conventional BET (Brunauer-Emmett-Teller) method from the adsorption isotherms in the relative pressure range of $P/P_0 = 0.04$-$0.2$. The total pore volume ($V_{total}$) was measured from the adsorbed $N_2$ amount at the relative pressure of 0.99. The pore size distribution was calculated by nonlocal density functional theory (NLDFT) using a carbon slit pore equilibrium model.

### Electrochemical measurements

To evaluate capacitive performance of the as-prepared activated carbon samples (~3-3.8 mg) in electrochemical capacitors, the electrode was fabricated from a blend of 80 wt% of the carbon sample, 10 wt% of carbon black and 10 wt% of binder polytetrafluoroethylene (PTFE) suspended in ethanol. Slurry of the above mixture was placed onto the nickel foam and subsequently pressed under a pressure of 20 MPa. The prepared electrode was placed in a vacuum drying oven at 120 ºC for 24 h. Electrochemical impedance spectroscopy (EIS), cyclic voltammetry (CV) and galvanostatic charge/discharge were recorded by using three electrodes experimental setup, in which 2 M KOH aqueous solution as electrolyte was used and operated by using CS350 electrochemical workstation (Corrtest, China) at the room temperature (25 ºC). The average specific capacitance was calculated from the galvanostatic discharge time curves, using the following equation:

$$C = \frac{I\Delta t}{m\Delta V}$$

Where C (F g$^{-1}$) is the specific capacitance, I (A) is the constant discharge current, $\Delta t$ (s) is a full discharge time, m (mg) is the mass of active materials loaded in working electrode, and $\Delta V$ (V) refers to the voltage change after a full discharge. Besides, specific energy density (E) and specific power density (P) derived from galvanostatic tests can be calculated using the following two equations:

$$E = \frac{1}{2}C\Delta V^2$$

$$P = \frac{E}{\Delta t}$$

Where E (W h kg$^{-1}$) is the average energy density, C (F g$^{-1}$) is the specific capacitance, $\Delta V$ (V) is the voltage change after a full discharge, P (W kg$^{-1}$) represent the average power density, and $\Delta t$ (s) is a full discharge time. [33]

Electrochemical Impedance System (EIS) was carried out from $10^6$ Hz to 0.01 Hz in a frequency sweep against the open circuit potential with a sinus amplitude of 10 mV (Vrms = 7.07 mV). The whole experimental process was repeated five times.

## Results

### Morphology of samples

The nitrogen-doped activated carbons, using conjugated polymer poly[(pyrrole-2, 5-diyl)-co-(benzylidene)] (PPCB) as precursor, were prepared by chemical activation at different temperature (700 °C and 800 °C) (Fig. 1).
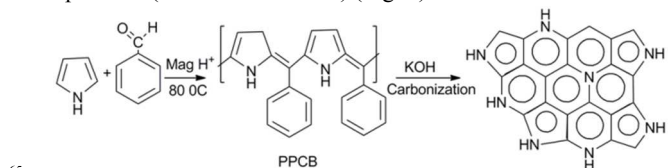


**Fig. 1** Schematic illustration of the preparation of Nitrogen -doped Activated Carbon (N-AC) Samples.
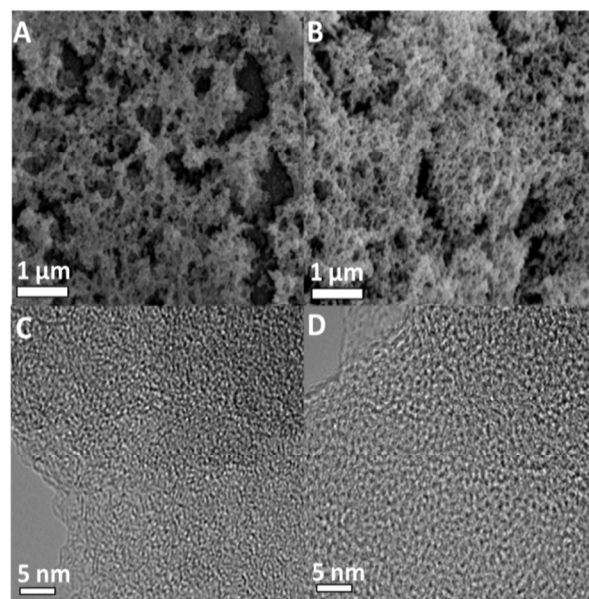


**Fig. 2** FE-SEM and HR-TEM images of samples: (A) and (C) N-AC-700; (B) and (D) N-AC-800.

Microstructural features of the N-ACs composites were examined by (FE-SEM) and (HRTEM). The representative FE-SEM images (Fig. 2 A and B) of the activated porous carbon indicate the presence of a holes with interconnected pores in a three-dimensional framework. This microporous structure is formed by chemical activation mechanism using KOH as a chemical activating agent. High resolution transmission electron microscopy (HR-TEM) (Fig. 2 C and D) demonstrates a uniform, large disorder microstructure, a slightly larger and less curved graphene segment produced at higher temperature, which is even

more clearly observed near the edges of the samples, where less sample thickness is generated by slight overlap between the randomly directed graphene layers. The irregular contrast in the HR-TEM images of the samples with varying thickness does not
5 provide a clear picture of pore size and their distribution. In spite of this, N-ACs reveal a high coordinated pores with a large fraction of micro and a little of mesopores, the overall structure consists of large micropores of an interconnected network, which is expected to give high permeability to transfer electrolyte ions
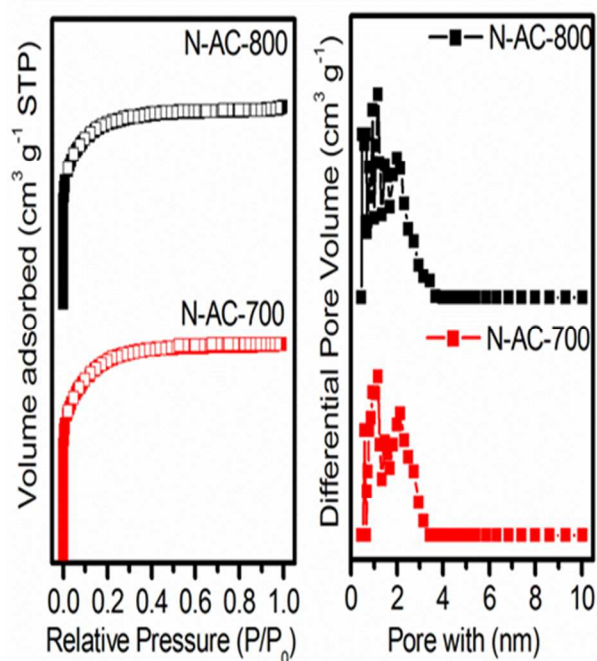10 through the pores.



**Fig. 3** $N_2$ adsorption/desorption isotherms and pore size distributions of the N-AC carbonized at different temperature.

15

It is known that KOH activation will introduce micro/mesopores structure into the resulting carbon whose surface area and porosity can be tuned by activation temperature. The textural properties of the different porous carbons at different
20 activation temperature (700 °C and 800 °C) were analyzed by means of $N_2$ adsorption at -196 ℃. The nitrogen sorption isotherms (Fig. 3) show that both samples exhibit a characteristic type I isotherm without any hysteresis loop, indicating the presence of a large number of micropores in AC samples. The
25 pore size distribution (PSD) calculated by the nonlocal density functional theory (NLDFT), assuming a slit geometry for micropores and a cylindrical pore geometry for the mesopores, reveals the existence of well-defined micro- and mesopores with sizes of less than 3 nm (Fig. 3). The specific surface area of N-
30 AC-800 is up to 2090 cm$^2$ g$^{-1}$, which is higher than N-AC-700 (1299 cm$^2$ g$^{-1}$) calculated in the P/P0 range 0.1.

The surface functional groups of the N-ACs are analyzed by Fourier Transform Infrared (FT-IR) spectroscopy, as shown in Fig 4. The broad band at 3440 cm$^{-1}$ is ascribed to the N-H stretching
35 vibrations, and the observed strong band at 1110 cm$^{-1}$ is attributed

to the C-N stretching vibrations. The small band at 1420 cm$^{-1}$ is assigned to the C=C backbone stretching vibrations, indicating the presence of aromatic groups. Finally, the vibration of the phenylene conjugated C=C and Cβ–H of the α-linkage in pyrrole
40 rings clearly appeared at 1638 cm$^{-1}$ and 740 cm$^{-1}$ for PPCB respectively whereas the disappearance of Cβ–H bands of N-AC samples indicated the elimination of hydrogen.[32] The chemical compositions of the N-AC materials were determined by using CHN elemental analyser. As shown in Table 1, the nitrogen
45 content decreases from 4.8 % to 4.1 % when the carbonization temperature increases from 700 °C to 800 °C. The N content in pure PPCB is 11.3 wt%, which is much higher than that in any N-ACs produced because a part of N was lost during carbonization and activation process.
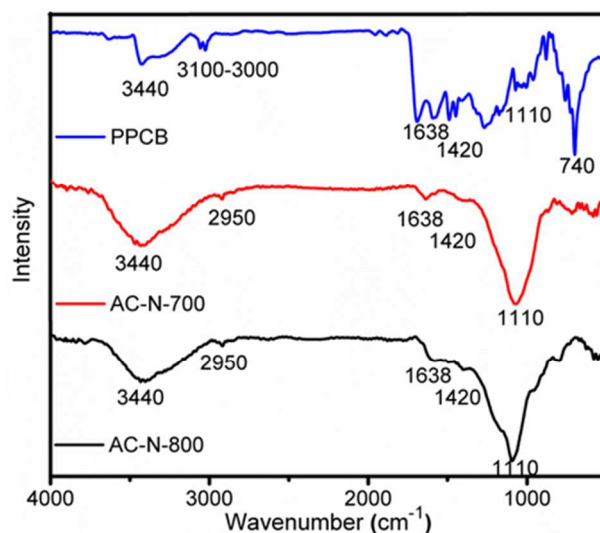


50
**Fig. 4** FT-IR Spectrum of the N-ACs samples.

**Table 1 Textural properties and elements analysis of N-ACs samples**

| Sample | $S_{BET}$ (m$^2$ g$^{-1}$) | Pore size (nm) | C% | N% | H% |
|---|---|---|---|---|---|
| **PPCB** | 139 | 4.3 | 84.4 | 11.3 | 4.2 |
| **N-AC-700** | 1299 | 2.0 | 93.5 | 4.8 | 2.2 |
| **N-AC-800** | 2090 | 1.9 | 94.1 | 4.1 | 1.7 |

55 To further confirm the structure of the as-prepared N-ACs samples, Raman spectrometer was used to study the structure. The Raman spectra of PPCB, N-AC-700 and N-AC-800 are shown in Fig. 5. All three curves exhibited the G-band centered at (ca.1590 cm$^{-1}$) corresponding to highly ordered graphite and
60 the D-band (ca.1345 cm$^{-1}$) originating from disordered carbon, which confirmed the formation of activated carbon. Also, the ratio of the D peak intensity to the G peak intensity ($I_D/I_G$) is generally used as a measure of the degree of defect of the activated carbon. $I_D/I_G$ ratios are 0.57, 0.89 and 9.90 for PPCB,
65 N-AC-700 and N-AC-800 respectively, revealing that the decrease of N-content would increase the degree of disorder in the final activated carbon structure.
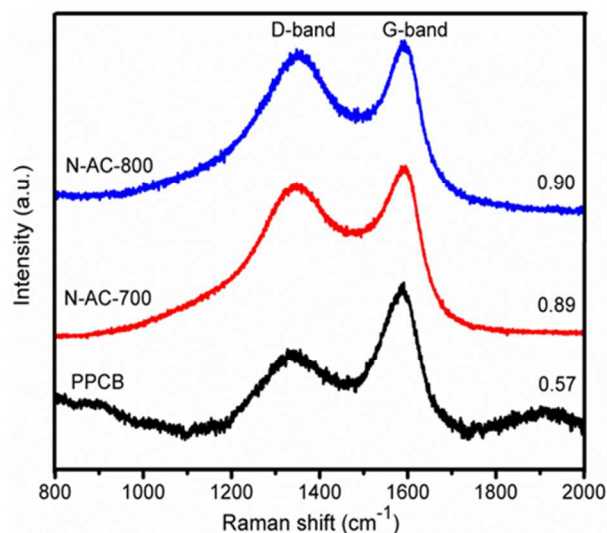
**Fig. 5** Typical Raman spectra of samples. The wavelength of Raman laser line is 522 nm.

5    Accordingly, the surface chemical properties of the as-prepared activated carbons were analysed using X-ray photoelectron spectroscopy (XPS) and the resulting spectra are shown in Fig. 6. XPS analysis reveals the bonding of N with C and the existence two types of N (N5 and N6). It shows that N-C bonding located at
10 400.1 eV was attributed to pyrrolic-N and a weak peak with binding energies centered at 388.7 eV and 399.2 eV for N-AC-700 and N-AC-800 respectively, indicating the presence of pyridinic-N. The total nitrogen contents in N-ACs were found to be inversely proportional to the activation temperature, indicating
15 that higher temperature will lead to more loss of nitrogen atoms during activation.

**Electrochemical capacitor behavior**

   The electrochemical capacitive performance of N-ACs was assessed by using a three-electrode method in electrolyte solution
20 (2M KOH). Fig. 7 (A-C) shows the cyclic voltammetry (CV) curves of porous carbon at scan rates from 5 to 100 mV s$^{-1}$ and the potential window range from -1 to 0 V). All the curves give a typical rectangular shape without any redox reaction. CV curves are well maintained at a low scanning rate of 5-20 mV s$^{-1}$,
25 indicating the perfect capacitive behaviour for both N-AC-700 and N-AC-800 electrodes. Nevertheless, when the scanning rate is changed to 50-100 mV s$^{-1}$, the shape of the CV curves manifests an increased deformation in the typical rectangular shape. Basically, these changes occur due to the following two
30 factors: at the higher scanning rate, there is no enough time for ions to move and accumulate, which leads to a decrease in an accessible surface area and an imperfect EDLC formation. Also at the higher scanning rate, the ohmic resistance is larger for ions movement in the pores, which impedes the EDLC formation,
35 when the EDLC is formed at lower scan rates, there is enough time for ions to diffuse towards the surface and the inner pores of the electrode materials.
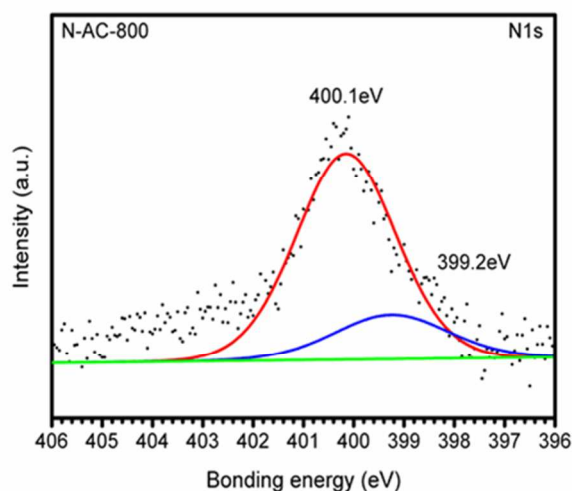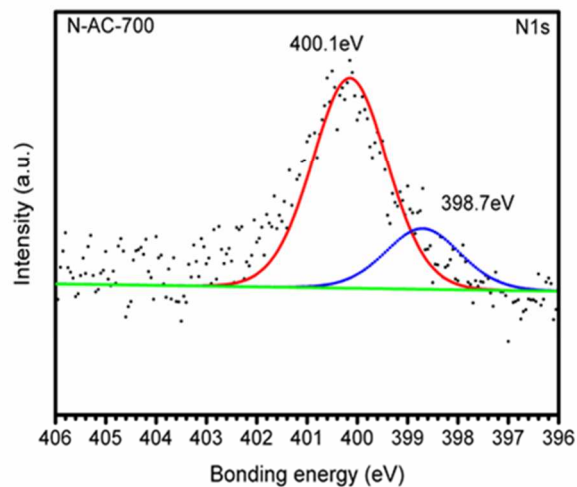




**Fig. 6** N1s line scan of N-AC samples, which confirms the presence of N
40 atoms (N5 and N6). The green line exhibits the Shirley background.

   Galvanostatic charge/discharge (GC) measurements were carried out to evaluate the electrochemical performance of the resulting samples (N-AC-700 and N-AC-800) as electrodes at the
45 current density of 0.16-3.33 A g$^{-1}$ in a 2 M KOH aqueous solution, with a potential window of -1 to 0 V. As shown in Fig. 8 (A and B), the GC curves of the N-AC-700 and N-AC-800 electrodes exhibit ideal isosceles triangle shapes, indicating that the charge time is equal to the discharge time. The electrodes
50 reveal a high reversibility. The symmetric charge/discharge curves in the voltage range available leading to the ideal EDLC behaviours were observed, which conform to the above CV measurements. The linear and symmetrical GC curves for N-AC-800 also reveal the excellent responses of electrode during the
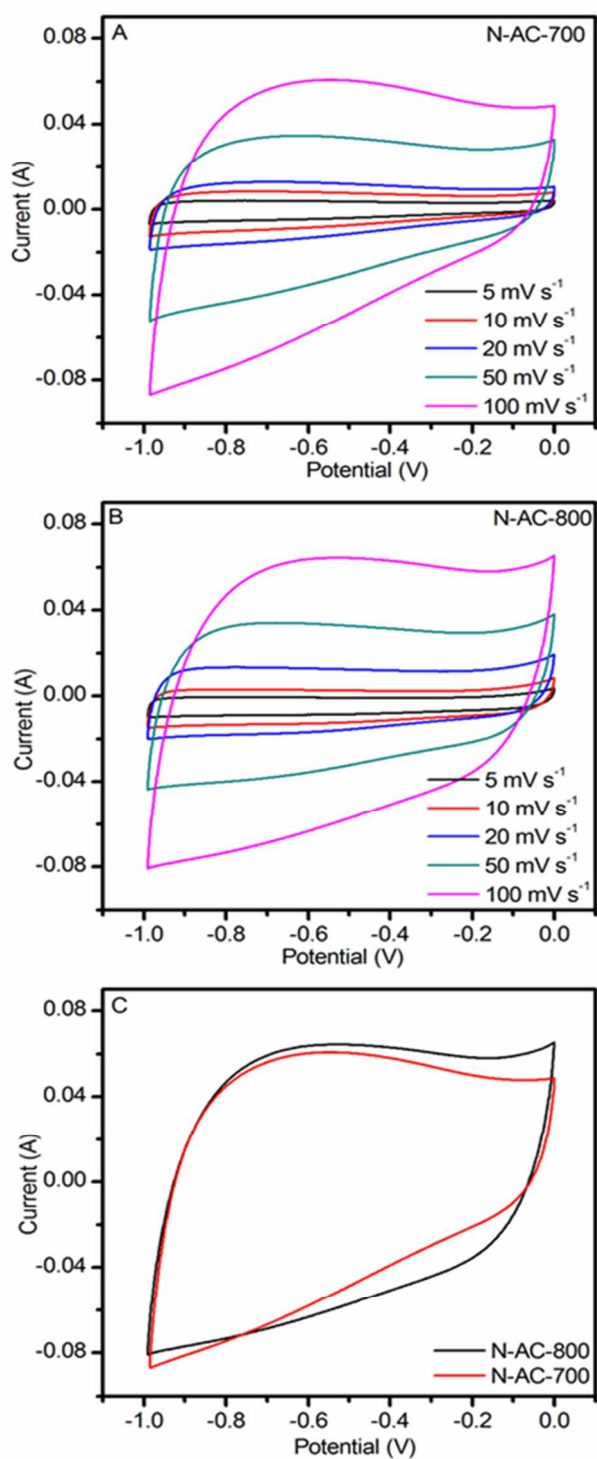55 whole potential range.

60

**Fig. 7** Cyclic Voltammetry (CV) curves of samples at different scan rates in 2M KOH. A) N-AC-700, B) N-AC-800 and C) CV of samples at scan rate 100mV s$^{-1}$.

The ACs electrodes have excellent electrochemical reversibility and Coulombic efficiency. The high-rate discharge features were assessed by controlling the nitrogen content at a suitable ratio through the choice of activation temperature, while the excessive nitrogen content can lead to a deteriorative rate performance.[34] Otherwise, the voltage drop (IR) at the beginning of the discharge curve is negligible for the N-AC-800, indicating small internal resistances for these electrodes.

The IR drop is 0.02 V at 0.33 A g$^{-1}$, 0.052 V at 0.66 A g$^{-1}$, 0.063 V at 1.66 A g$^{-1}$ and 0.94 V at 3.33 A g$^{-1}$ for N-AC-700 sample, signifying the IR drop reduction with the decreasing current density as is shown in Fig. 8 A and C. It is generally recognized that the IR drop is related to the electrical conductivity and porous structure of the electrode. Specimen N-AC-800 has the lowest IR drop due to a combination of the highest electrode conductivity and the optimum porous structure.

A higher specific capacitance (C$_{sp}$) of the ACs electrode is calculated according to the discharge time (525.5 F g$^{-1}$ for N-AC-800 electrode at current density 0.26 A g$^{-1}$ and 491 F g$^{-1}$ for N-AC-700 electrode at current density 0.16 A g$^{-1}$). The open micropores increase the surface area and small pore volume (1299-2042 m$^2$ g$^{-1}$ and 0.376-0.742 cm$^3$ g$^{-1}$) which enhances the electrochemical properties. The presence of active N atoms on the electrode surface supports the charge transfer and minimise the ion diffusion distance during the charge-discharge process. Moreover, abundant micropores were found in the carbon matrix (Fig. 2 A and B), which provide regular and proper interconnecting pathways for the mobility of atoms and ions through the pore channels, thereby contributing towards improving the capacitance of the capacitors comprising of such electrodes.[35] When the current density increases to an ultrahigh density of 100 A g$^{-1}$, the specific capacitance of A-NC-800 electrode can be retained to 390 F g$^{-1}$. The obtained results clearly demonstrate the effectiveness of well-connected porous carbon structure for improving electrolyte accessibility and electrical conductivity.

The electrochemical features are better manifested by the EIS measurement. Fig. 8 D is a Nyquist plot of the N-AC-700 and N-AC-800 in the same electrolyte and identical frequency range, which shows similar curves including a small semicircle at the high frequency and an inclined line at the low frequency. The intercept at the X-axis refers to solution resistance (Rs), which comprises the essential resistance of the porous materials, the resistance of the electrolyte solution, and the contact resistance at the interface between active porous materials and current collectors. The charge transfer resistance (Rct) is displayed by the diameter of the semicircle on the X- axis in the electrochemical system at the low-frequency region. However, R$_s$ and R$_{ct}$ for N-AC-800 (0.16 Ω and 0.61 Ω) are both smaller than those of N-AC-700 (0.37 Ω and 0.74 Ω). This tendency line is absolutely parallel to the electrochemical activities shown by the charge-discharge measurements. The specific capacitance (C$_{sp}$) is found to be 525.5 F g$^{-1}$ at 0.26 A g$^{-1}$ and retains 74% of this value (390 F g$^{-1}$) at increasing current density to 26.31 A g$^{-1}$ (Fig. 9 A). These results indicate that the interconnected micro/mesopores structure demonstrates an efficient pathway for electrolyte ion movement through the carbon matrix.
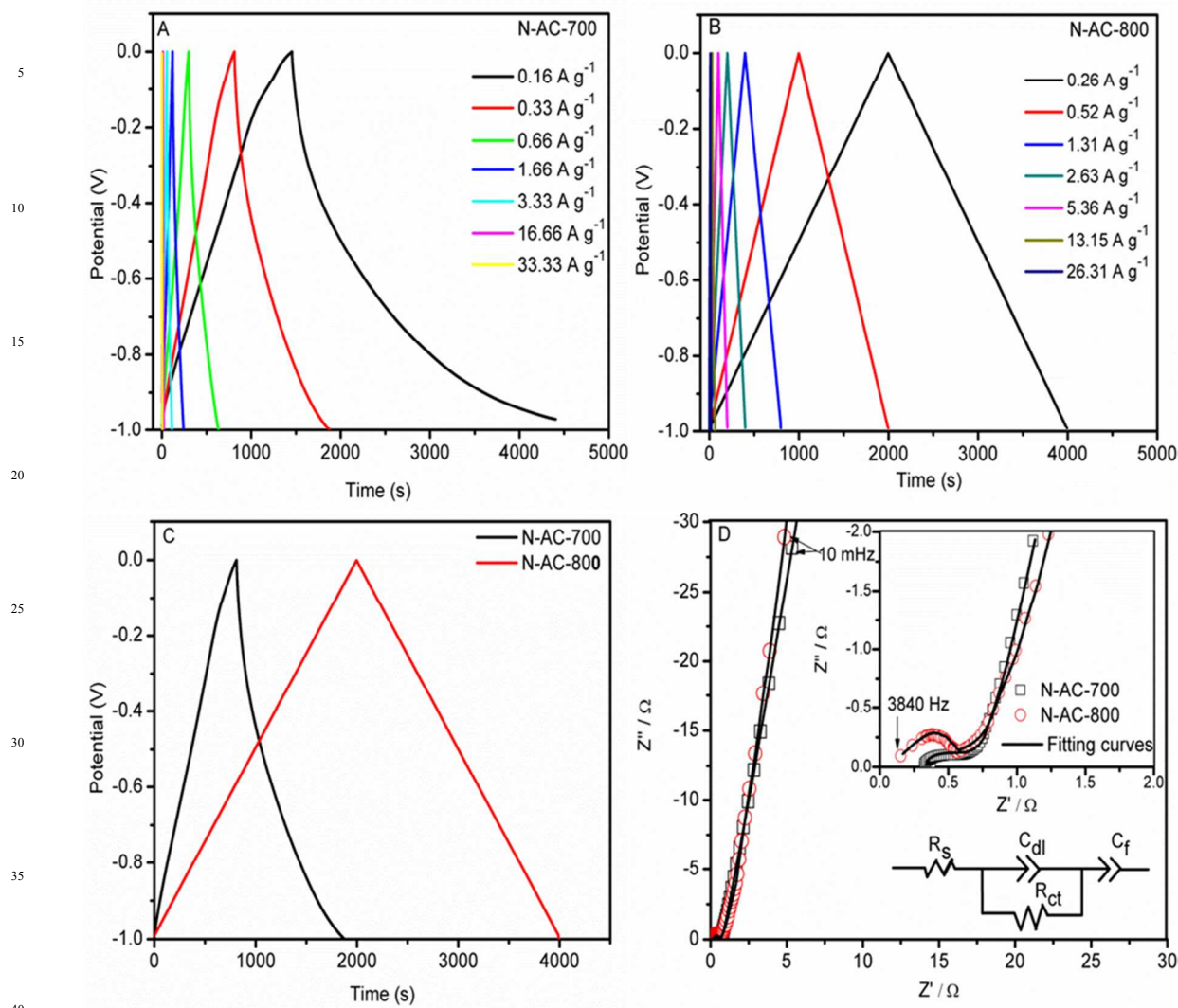
**Fig. 8** Galvanostatic charge/discharge (GC) curves of samples A) N-AC-700, B) N-AC-800 at different current density with 2M KOH. C) GC at current density 0.26A g-1. D) Nyquist plots for the (black) N-AC-700 and the (red) N-AC-800 composites in the same electrolyte. Insets are plots at high-frequency region and the equivalent circuit used to fit the impendence spectra.

For practical applications of electrochemical supercapacitors, the stability of long cycling is a crucial factor. Here, the stability of long-term cycling stability with 4000 charge/discharge cycles of activated carbon is depicted by Ragone plots (Fig. 9 B). The capacitance retention almost keeps constant (Even after 4000 charging/discharging cycles about 99.5% of N-AC-800 electrode at current density of 0.26 A $g^{-1}$ and 99% of N-AC-700 electrode at 0.33 A $g^{-1}$) with a slight variation. The cycling performance is better than that of the previously reported activated carbons, such as (Catechol,[36] RAC, [37] AC-800, AC400,[38] and a MEGO).[39] These results reveal the unique capability of the N-ACs electrode to satisfy the conditions for large capacitance and long cycling life.

In addition, energy (E) and the power (P) density are also important parameters to evaluate the electrochemical properties of supercapacitors. These are calculated from galvanostatic charge/discharge values, as show in Fig. 9 C. It is clearly evident that the energy density of N-AC composites increases with the scan rate decreasing, contrary to the specific power density value. The highest energy density is 262.7 W h $kg^{-1}$ at a power density of 131 W $kg^{-1}$ for N-AC-800 electrode, and it remained at 195 W h $kg^{-1}$ when the power density is elevated to 10.8 KW $kg^{-1}$. These values are higher than those of N-AC-700 electrode and previously reported ACs based electrode materials.
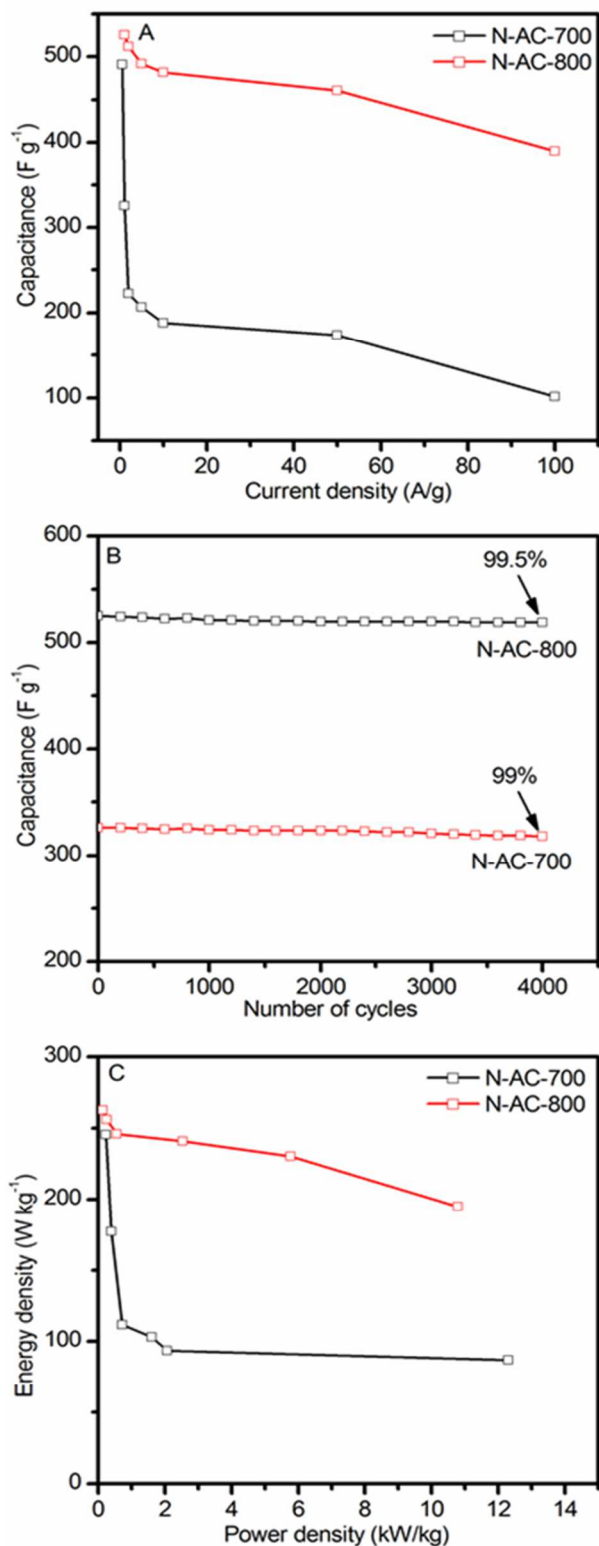
**Fig. 9** A) Specific Capacitance ($C_{sp}$) of N-ACs electrode at various scanning rates , B) Cycling stability of samples at current density 0.26 A $g^{-1}$ for N-AC-800 electrode and N-AC-700 at current density 0.33 A $g^{-1}$, C) Ragone plot ( energy density vs power density) all measurements in 2 M KOH electrolyte solution.

## Conclusion

In summary, N-ACs prepared by graphitization of the PBCP as a precursor, show an increased specific surface area, an improved pore volume and a pore size, which are indeed essentially required for a higher supercapacitor performance. Moreover, N-ACs could be one of the best candidates for supercapacitors with a high specific capacitance of 525.5 F $g^{-1}$ and a large energy density of 262.7 W h $kg^{-1}$ due to their superior properties such as recyclability and smaller inner resistance as well as higher electrical conductivity due to their exquisite microstructure and adequate nitrogen content. These encouraging results indicate the potential for possible future electrochemical energy storage applications.
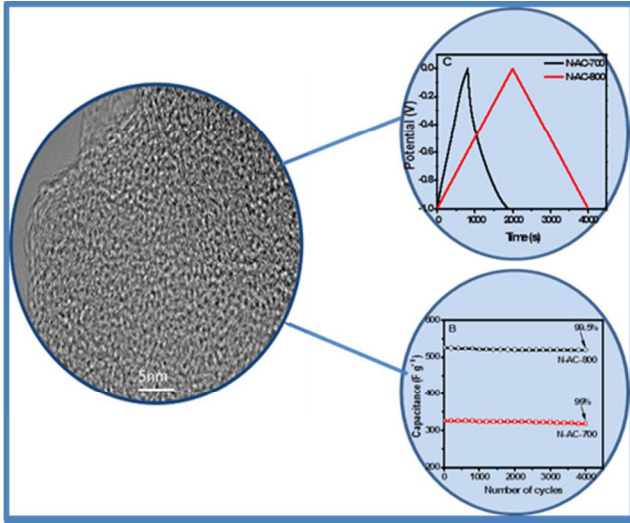
## Acknowledgement

## Notes and references

*a Hubei Key Laboratory of Material Chemistry and Service Failure, Key Laboratory for Large-Format Battery Materials and System, Ministry of Education,, school of Chemistry and Chemical Engineering, Huazhong University of Science and Technology, Wuhan, P.R. China.*
*E-mail: bien.tan@mail.hust.edu.cn; Fax: +86 27 87543632; Tel: +86 27 87558172*
*b South refineries company, ministry of oil, Basra, Iraq.*
*c Institute of Superconducting & Electronic Materials, The University of Wollongong, NSW 2500, Australia. Fax: +61-2-42215731; E-mail: zhenl@uow.edu.au*

1. L. Nyholm, G. Nystrom, A. Mihranyan and M. Stromme, *Advanced Materials*, 2011. **23**, 3751-3769.
2. Y. S. Yun, S. Y. Cho, J. Shim, B. H. Kim, S. J. Chang, S. J. Baek, Y. S. Huh, Y. Tak, Y. W. Park, S. Park and H. J. Jin, *Advanced Materials*, 2013, **25**, 1993-1998.
3. J. Wang, Y. Xu, F. Yan, J. Zhu and J. Wang, *Journal of Power Sources*, 2011, **196**, 2373-2379.
4. Y. Song, D. Zhou, Y. Wang, C. Wang and Y. Xia, *New Journal of Chemistry*, 2013, **37**, 1768-1775.
5. J. Chmiola, G. Yushin, Y. Gogotsi, C. Portet, P. Simon and P. L. Taberna, *Science*, 2006, **313**, 1760-1763.
6. S. Dhibar, S. Sahoo and C. K. Das, *Journal of Applied Polymer Science.*, 2013, **130**, 554-562.
7. T.-c. Chou, C.-h. Huang, R.-a. Doong and C.-c. Hu, *Journal of Materials Chemistry A*, 2013, **1**, 2886-2895.
8. X. Wen, D. Zhang, T. Yan, J. Zhang and L. Shi, *Journal of Materials Chemistry A*, 2013, **1**, 12334-12344.
9. Z. Weng, F. Li, D. W. Wang, L. Wen and H. M. Cheng, *Angewandte Chemie*, 2013, **52**, 3722-3725.
10. P. Yu, Y. Li, X. Yu, X. Zhao, L. Wu and Q. Zhang, *Langmuir: the ACS Journal of Surfaces and Colloids*, 2013, **29**, 12051-

12058.

11.   M. Liu, Y. E. Miao, C. Zhang, W. W. Tjiu, Z. Yang, H. Peng and T. Liu, *Nanoscale*, 2013, **5**, 7312-7320.

12.   A. Kumar, R. Singh, K. Agarwal, H. Singh, P. Srivastava and R. Singh, *Journal of Applied Polymer Science*, 2013, **130**, 434-442.

13.   F. Zhang, F. Xiao, Z. H. Dong and W. Shi, *Electrochimica Acta*, 2013, **114**, 125-132.

14.   J. Hu, P. Tao, S. Wang, Y. Liu, Y. Tang, H. Zhong and Z. Lu, *Journal of Materials Chemistry A*, 2013, **1**, 6558-6562.

15.   L. Chen, X. Zhang, H. Liang, M. Kong, Q. Guan, P. Chen, Z. Wu and S. Hong, *ACS NANO*, 2012, **6**, 7092-7102.

16.   R. Liu, D. Wu, X. Feng and K. Mullen, *Angewandte Chemie*, 2010, **49**, 2565-2569.

17.   H. Feng, B. Wang, L. Tan, N. Chen, N. Wang and B. Chen, *Journal of Power Sources*, 2014, **246**, 621-628.

18.   Y. Cui, Q. Y. Cheng, H. Wu, Z. Wei and B. H. Han, *Nanoscale*, 2013, **5**, 8367-8374.

19.   T. Ren, Y. Si, J. Yang, B. Ding, X. Yang, F. Hong and J. Yu, *Journal of Materials Chemistry*, 2012, **22**, 15919-15927.

20.   S. Palaniappan, S. B. Sydulu and P. Srinivas, *Journal of Applied Polymer Science*, 2010, **115**, 1695-1701.

21.   B. Xu, S. Hou, G. Cao, F. Wu and Y. Yang, *Journal of Materials Chemistry*, 2012, **22**, 19088-19093.

22.   L. Zhang, T. Lin, X. Pan, W. Wang and T.-X. Liu, *Journal of Materials Chemistry*, 2012, **22**, 9861-9869.

23.   D. Zhou, W.-Y. Li, X.-L. Dong, Y.-G. Wang, C.-X. Wang and Y.-Y. Xia, *Journal of Materials Chemistry A*, 2013, **1**, 8488-8496.

24.   Y. Liu, B. Zhang, Y. Yang, Z. Chang, Z. Wen and Y. Wu, *Journal of Materials Chemistry A*, 2013, **1**, 13582-13588.

25.   W. Liu, X. Yan, J. Chen, Y. Feng and Q. Xue, *Nanoscale*, 2013, **5**, 6053-6062.

26.   Y. Tan, C. Xu, G. Chen, Z. Liu, M. Ma, Q. Xie, N. Zheng and S. Yao, *ACS Applied Materials & Interfaces*, 2013, **5**, 2241-2248.

27.   L. Estevez, R. Dua, N. Bhandari, A. Ramanujapuram, P. Wang and E. P. Giannelis, *Energy & Environmental Science*, 2013, **6**, 1785-1792.

28.   M. Ingram, *Solid State Ionics*, 2004, **169**, 51-57.

29.   S. Sahoo, S. Dhibar, G. Hatui, P. Bhattacharya and C. K. Das, *Polymer*, 2013, **54**, 1033-1042.

30.   T. Qian, C. Yu, S. Wu and J. Shen, *Journal of Materials Chemistry A*, 2013, **1**, 6539–6542.

31.   J.-H. Kim, Y.-S. Lee, A. K. Sharma and C. G. Liu, *Electrochimica Acta*, 2006, **52**, 1727-1732.

32.   A. Belmokhtar, *eXPRESS Polymer Letters*, 2007, **1**, 443-449.

33.   Y. Wang and Y. Xia, *Advanced Materials*, 2013, **25**, 5336-5342.

34.   L. Qie, W. Chen, H. Xu, X. Xiong, Y. Jiang, F. Zou, X. Hu, Y. Xin, Z. Zhang and Y. Huang, *Energy & Environmental Science*, 2013, **6**, 2497-2506.

35.   P. K. Tripathi, M. Liu, Y. Zhao, X. Ma, L. Gan, O. Noonan and C.Yu, *Journal of Materials Chemistry A*, 2014. DOI: 10.1039/c4ta00578c.

36.   G. Pognon, C. Cougnon, D. Mayilukila and D. Bélanger, ACS *Applied Materials & Interfaces*, 2012, **4**, 3788−3796.

37.   M. H. Kim, K. B. Kim and c. J. T. H. a. K. C. R. b Kisuk Kang, *Journal of Materials Chemistry A*, 2013, **1**, 14008-14012..

38.   M. Zhang, X. Jin, Y. Wu, *Wood Research*, 2013, **58**, 81-90.

39.   S. Murali, N. Quarles, Li, Zhang, J. R. Potts, R. S. Ruoff, *Nano Energy*, 2013, **2**, 764-768.

**TOC**



5